LD-CNV: rapid and simple discovery of chromosomal translocations using linkage disequilibrium between copy number variable loci

Luca Comai*, Kirk Amundson*, Benny Ordonez*, Xin Zhao*[,%], Guilherme Tomaz Braz[†], Jiming Jiang[†,#], Isabelle Henry*

*Plant Biology and Genome Center, University of California, Davis, California 95616, †Department of Plant Biology, [#]Department of Horticulture, Michigan State University, East Lansing.

[%]Current address: Institute of Vegetables and Flowers, Chinese Academy of Agricultural Sciences, Beijing

ORCID IDs: 0000-0003-2642-6619 (L.C.); 0000-0003-3435-626X (K.R.A.); 0000-0003-4554-4354 (B.O.); 0000-0002-6435-6140 (J.J), 0000-0002-6796-1119 (I.M.H.)

Correspondence: Luca Comai, lcomai@ucdavis.edu

Abstract

Large scale structural variations, such as chromosomal translocations, can have profound effects on fitness and phenotype, but are difficult to identify and characterize. Here, we describe a simple and effective method aimed at identifying translocations using only the dosage of sequence reads mapped on the reference genome. We binned reads on genomic segments sized according to sequencing coverage and identified instances when copy number segregated in populations. For each dosage-polymorphic 1Mb bin, we tested linkage disequilibrium (LD) with other variable bins. In nine potato (*Solanum tuberosum*) dihaploid families translocations affecting pericentromeric regions were common and in two cases were due to genomic misassembly. In two populations, we found evidence for translocation affecting euchromatic arms. In cv. PI 310467, a non-reciprocal translocation between chromosome 7 and 8 resulted in a 5-3 copy number change affecting several Mb at the respective chromosome tips. In cv. "Alca Tarma", the terminal arm of chromosome 4 translocated to the tip of chromosome 1. Using oligonucleotide-based fluorescent in situ hybridization painting probes (oligo-FISH), we tested and confirmed the predicted arrangement in PI 310467. In 192 natural accessions of *Arabidopsis thaliana*, dosage haplotypes tended to vary continuously and resulted in higher noise, while LD between pericentromeric regions suggested the effect of repeats. This method should be useful in species where translocations are suspected because it tests linkage without the need for genotyping.

Introduction

Genomic structural variation (SV) is common within plant populations (Swanson-Wagner *et al.* 2010) and has a profound effect on the phenotype of individuals (Díaz *et al.* 2012; Maron *et al.* 2013; Bastiaanse *et al.* 2019). SV is manifested at multiple scales, from single genes to large chromosomal regions, such as variable heterochromatic blocks in the pericentromeres of potato (*Solanum tuberosum*) (Gong *et al.* 2012; Zhang *et al.* 2014; de Boer *et al.* 2015; Hardigan *et al.* 2016). Small scale SV can alter gene structure and copy number. Large scale translocations and inversions can alter copy number, recombination, meiotic anaphase patterns, viability of gametes, gene structure, and evolutionary potential (Khush 1973; Rieseberg 2001). Translocations, which tend to be underdominant, i.e. to confer a heterozygous disadvantage (Rieseberg 2001), can persist in nature when they involve reciprocal exchanges of chromosome arms, resulting in copy-neutral, monocentric recombinant chromosomes. Nonreciprocal translocations are often deleterious because they can involve duplication and deletion of segments of the recombined chromosomes. However, in polyploids their effect is lessened by genomic redundancy.

Detection of translocation is not simple and often requires multiple approaches. SV loci display linkage disequilibrium (LD) with linked regions (Hinds *et al.* 2006; Locke *et al.* 2006). Translocations were originally detected by observing unusual lethality and unexpected linkage in Drosophila (Bridges 1923) and in plants (Belling and Blakeslee 1924). Later, they were confirmed cytologically (Belling and Blakeslee 1924; Muller 1929; McClintock 1930; Burnham 1956). The development of fluorescent in situ hybridization (FISH) facilitated their identification because each chromosome in a spread could be identified by cytological markers or by chromosome painting (He *et al.* 2018). Detection by FISH analysis requires chromosome-specific probes (Cremer *et al.* 1988), which can be readily developed using an oligonucleotide-based methodology (Zhang *et al.* 2021).

Genome sequencing can be informative of copy number changes and novel junctions (Alkan *et al.* 2011). Dosage analysis of sequence reads is informative when unbalanced translocations result in copy number variation (CNV), and when balanced translocations generate copy number variable progeny. CNV can be inferred by count of genomic sequencing reads. Regions with high or low read counts have likely undergone duplication or deletion. Read count, however, does not provide information on the context and position of copy number variable regions. Specifically, a duplication could involve transposition or be in tandem. The software CNVmap exploits heterozygous states arising from duplications to detect and map CNV (Falque *et al.* 2019). However, SNP between duplicated loci is a function of duplication age and may not be present in newly arisen structural variation. Evidence of a junction between two different chromosomes can be obtained by detecting sequencing reads that directly or indirectly span the junction. In

practical terms, however, identification and characterization of a translocation is not simple, particularly in the absence of prior evidence pointing to its location. DNA analysis is complicated by the presence of many spurious signals in mapped sequenced reads, especially when using short sequencing reads, and by the frequent presence of repetitive DNA at translocation junctions (Chen *et al.* 2010). Long read technology can be effective at addressing these problems (Sedlazeck *et al.* 2018), although it is typically more expensive than short read sequencing.

Polyploid species are more likely to display large SV because their genome buffers the deleterious effects of copy number changes (Comai 2005). In polyploids, gametes carrying a large chromosomal deletion might still be viable because they carry a second normal copy of the affected chromosome. Cultivated potato is an autotetraploid, highly heterozygous organism that is clonally propagated, but capable of elevated outcrossing rates (Brown 1993). The potato genome displays a high density of nucleotide and structural polymorphism, suggesting high plasticity (Hardigan *et al.* 2016, 2017). From a cultivated tetraploid potato clone, sexual haploid progeny can be extracted by pollination with a haploid inducer (Fig.1-A). These haploids inherit a diploid genome consisting of the maternal gametic contribution and are therefore called dihaploids. Their diploid genome simplifies genetic analysis. Further, they are fertile when crossed to many wild diploid accessions, enabling the bridging of germplasm and introduction of valuable traits into cultivated potato (Peloquin *et al.* 1989; Rokka 2009).

To investigate structural genomic variation, we developed a novel translocation detection approach and demonstrated its application in potato. Our method does not require genotyping or prior identification of polymorphism, such as SNPs or other common genetic markers. Instead, it leverages the reference genome sequence and dosage states inferred from sequencing the genome of related individuals, such as dihaploids of the same parent, in order to identify LD between structurally variant loci. The resolution of the identified structural variation scales with sequencing coverage, but even low coverage data can lead to interesting findings. Using several potato dihaploid populations, we demonstrate discovery of translocations in two families, as well as regions that could either be translocated and polymorphic, or assembly errors.

Results

Identification and LD analysis of CNV loci in a dihaploid population of potato

We generated a family of different ploidy types by crossing tetraploid potato variety PI 310467 to haploid inducer IvP48, producing a population called BB (Fig.1-A). PI 310467 is listed as Desiree in the GRIN germplasm collection but, although related, it differs from Desiree in its SNP profile (K.A., unpublished results). In the BB progeny, we selected and analyzed 84 2X haploids (dihaploids) by flow cytometry and low-pass genome sequencing. For comparison, we

also analyzed 78 4X hybrid siblings. Mapped reads were counted in non-overlapping, 1Mb genomic intervals along the reference genome, and these counts were standardized to a mean of 2 using the corresponding maternal variety counts. When these standardized dosage values from all individuals were overplotted, CNV polymorphisms were readily visible, as displayed for chr.1 (Fig. 1, Suppl. Fig. 1). Invariant regions form unimodal distributions, while polymorphic regions form bimodal or multimodal distributions (Fig.1-BC). For each of these regions, individuals could be clustered based on their corresponding read counts (Fig.1-D, Suppl. Fig.1, Suppl. Fig.2). We used the Python utility Peakutils (Negri) to identify these clusters and assign each individual to a genomic dosage state, which can be viewed as a stepwise, quantitative phenotype resulting from additive alleles.

Consistent with previous reports (de Boer *et al.* 2015; Hardigan *et al.* 2016; Amundson *et al.* 2020a), dosage variation was common in pericentromeric regions (Fig.1-B, Suppl. Fig.1). To further characterize the associated structural changes, we asked whether dosage variation at different loci was independent. Linked loci, such as those in the same pericentromeric regions, would be expected to co-vary, i.e. to exhibit LD. Dosage states of unlinked loci should be independent. Unexpected LD suggests either epistasis or novel linkage, such as resulting from a translocation or genome assembly error. Therefore, for each SV locus, we tested the null hypothesis that its dosage states were independent of dosage states at another SV locus (Fig. 2).

After correction for multiple testing (Benjamini and Hochberg 1995), associations between bins were plotted on a genomic matrix (Fig. 3). The potato genome was partitioned in 731 1Mb bins, of which 246 (33% of genome) displayed distinct dosage states. Most, 236, were in LD with at least another bin (corrected $p < 0.05$). This is not surprising, since LD is expected for physically linked loci. However, 65 bins were in LD with bins on other chromosomes, indicating that 26.7% of copy variable sequences display unexpected linkage. Loci in LD detected with FDR = 0.05 are marked in blue and black in the matrix (Fig. 3).

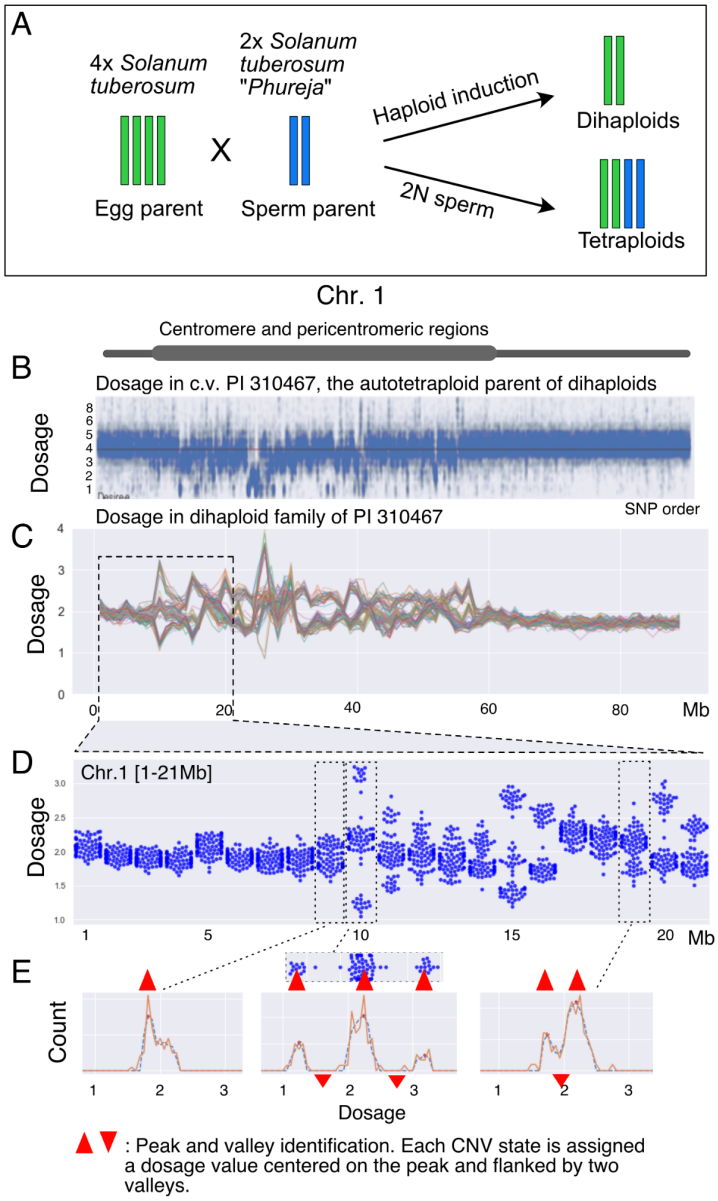

Figure 1. Dosage states of potato chromosome 1 in 84 dihaploid siblings.
A. Haploid induction crosses generate progeny of different ploidy. Dihaploids inherit the genomic content of the egg gamete exclusively. Tetraploids are hybrids and receive contribution from both parental genomes. Triploid hybrids are also possible, but not depicted or analyzed here. B. Standardized coverage per SNP of chromosome 1 for the tetraploid parent PI 310467. C. Relative dosage states along chr.1 were derived by sequence coverage binned on 1Mb intervals and standardized on the maternal dosage. 84 maternal dihaploid individuals produced from the haploid induction cross *S.t.* PI 310467 x *S.t. group phureja* IvP48 are overplotted revealing recurring dosage trends and polymorphism, mainly associated with heterochromatic regions along the pericentromere. D. Swarm plots of dosage states in the first 21 Mb of chr.1. E. Cluster derivation by Peakutils. Peaks (upward red arrowheads) are identified by the algorithm, while valleys (downward red arrowheads) are defined as the mid distance between peaks. Dosage values flanked by two valleys were assigned to the corresponding clusters.

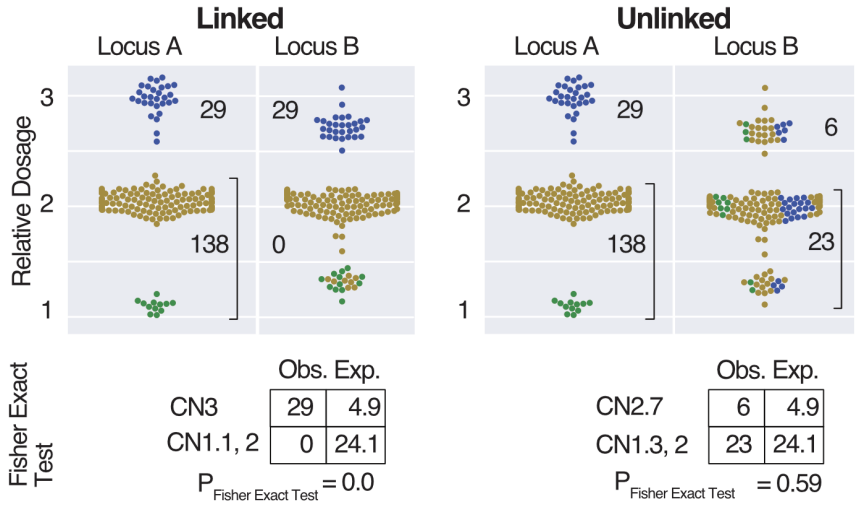

Figure 2. Testing random association between dosage states at different loci.
Hypothetical loci A and B are illustrated for linked (left) and unlinked (right) states. The independence test compares dosage states at the two loci. Here, the top cluster is compared to the aggregate of the other two, producing a Fisher Exact 2x2 contingency table. Obs. = observed, Exp. = expected according to random association.

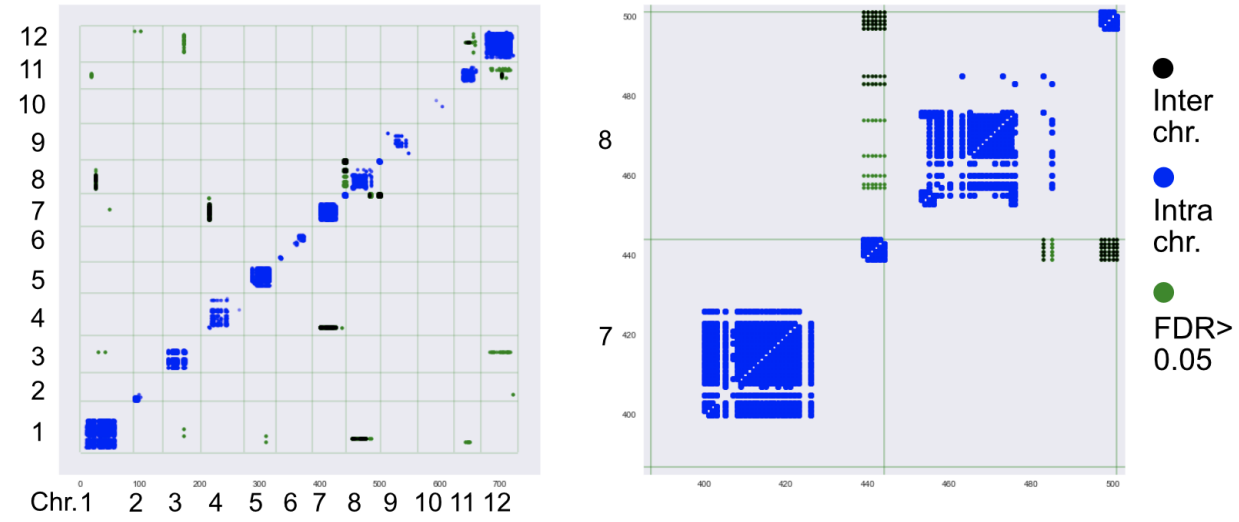

Figure 3. LD matrix of genomic dosage relationships.
A twelve chromosome matrix on the left displays significant interactions (Fig. 2), with a zoomed view on two chromosomes on the right. Note that only CNV loci can be tested. To illustrate that most interactions are statistically significant, green dots illustrate the relatively few interactions for which Fisher Exact $p < 0.05$, but that did not pass the multiple test correction. Black and green (interchromosomal), blue (intrachromosomal).

The Fisher Exact matrix displays the expected correlation between loci linked in cis, as a diagonal line and blocks that correspond to low recombination intervals positioned around the centromeres (Fig. 3). In addition to intrachromosomal interactions, cases of strong interchromosomal ones are evident, suggesting physical linkage. For example, a region of 1Mb in chromosome 1 displays an association to the entire pericentromeric region of chromosome 8. Similar interactions are visible between chr. 4 and chr. 7 and between chr. 11 and chr. 12. These could be translocated heterochromatic blocks, which have been demonstrated in potato (Zhang *et al.* 2014; de Boer *et al.* 2015), or genomic assembly errors (see below).

An alternative approach to determining Fisher Exact probabilities, is correlation based on Pearson's R., which while less sensitive and less interpretable could often provide equivalent information because translocation signals are strong (Methods; Suppl. Fig. 3, Suppl. Fig. 4).

Translocation of a euchromatic 6Mb region between chr. 7 and 8

We noted a strong signal between the 6Mb euchromatic right arm of chr. 7 and the 5Mb right arm of chr. 8 (Fig. 3). In the dosage plots (Fig. 4), both chromosomes display distinct copy number polymorphism with absolute correlation between dosage states: higher dosage of chr. 7 was always associated with lower dosage of chr. 8. Translocation of the terminal segment of chr. 7 to chr. 8 with concurrent loss of the 5Mb terminal region of 8 (Fig. 4-B) could explain the observations, as illustrated in the inheritance and dosage model (Fig. 4-B, Suppl. Fig. 2). The dosage plots in Fig. 4 were constructed by standardizing read counts to those of parent variety PI 310467, i.e. they are relative to the control. To test the above hypothesis, we plotted raw genomic dosage of putative single copy regions corresponding to SNP (Fig. 5-C, blue track) (see Methods). We also used SNP count ratios to provide an independent measure of copy number. Fig. 5-B,C demonstrates that there are 5 copies for chr. 7 and three copies of chr. 8 in the involved regions. To provide conclusive validation for this translocation, we conducted FISH using two oligonucleotide-based chromosome painting probes specific for chr. 7 and chr. 8, respectively (Fig. 5). We observed four normal copies of chr. 7 and three normal copies of chr. 8. One additional copy of chr. 8 carried a region of chr. 7 (Fig. 5D). We concluded that the PI 310467 clone has an unbalanced translocation between chr. 7 and chr. 8. The presence of this translocation was verified by obtaining and sequencing a second, independent sample of PI 310467 from the USDA Potato Genebank (data not shown).

In summary, analysis of covarying dosage states identified regions in linkage disequilibrium (i.e. genetically linked) including the unbalanced translocation between chr. 7 and chr. 8.

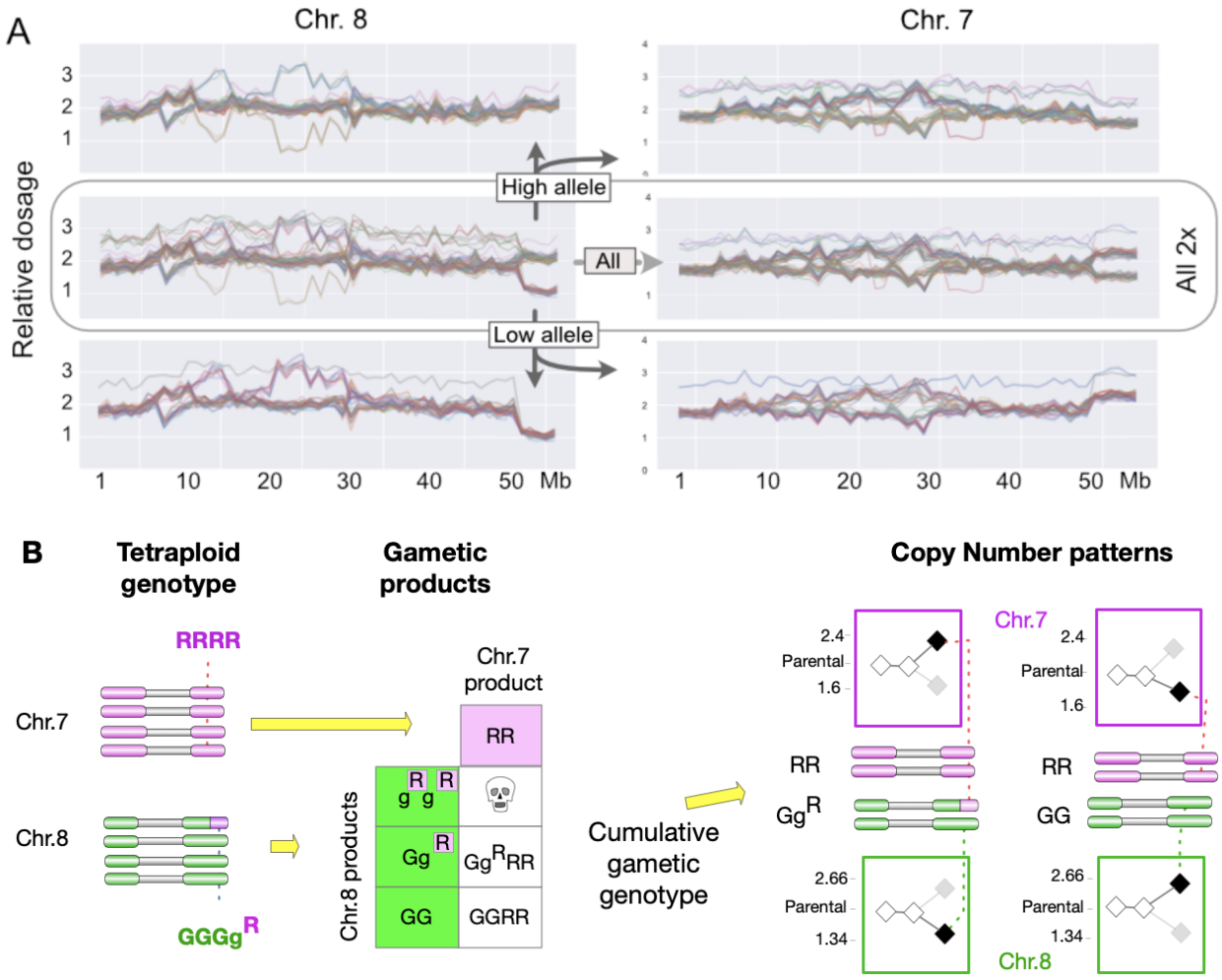

Figure 4. Analysis of CNV states in chromosome 7 and 8 of potato clone PI 310467.
A. Complete correlation of CNV state between chr. 8 and chr. 7 in the population of dihaploids. Chr. 8 and chr. 7 relative dosages are plotted using all 2x individuals (center row) or filtered sets (top and bottom row), relative to the parental genome of PI 310467. High allele: Selection of individuals where chr. 8 distal right arm copy number > 1.5. Trisomic individuals (high dosage tracks) are removed. Low allele: Selection of individuals where chr. 8 distal right arm copy number < 1.5. The dosage of each individual was calculated by dividing standardized reads per bin by the corresponding count for PI 310467. The dosage shown is therefore not absolute, but relative to that of the maternal dosage. B. Model of Tr.8-7 in autotetraploid Alca Tarma (a.k.a. LOP868), meiotic transmission pattern of chr. 7 and chr. 8 into gametes. On the right, the genotype of dihaploids is displayed together with the resulting copy number pattern for the terminal, right arm region of chr. 7 and chr. 8. The values are relative. For example, the terminal region of 7 is present in 3 copies in the RRGg^R dihaploid and 5 in the tetraploid parent. The relative dosage = 3/5 * 4 = 2.4

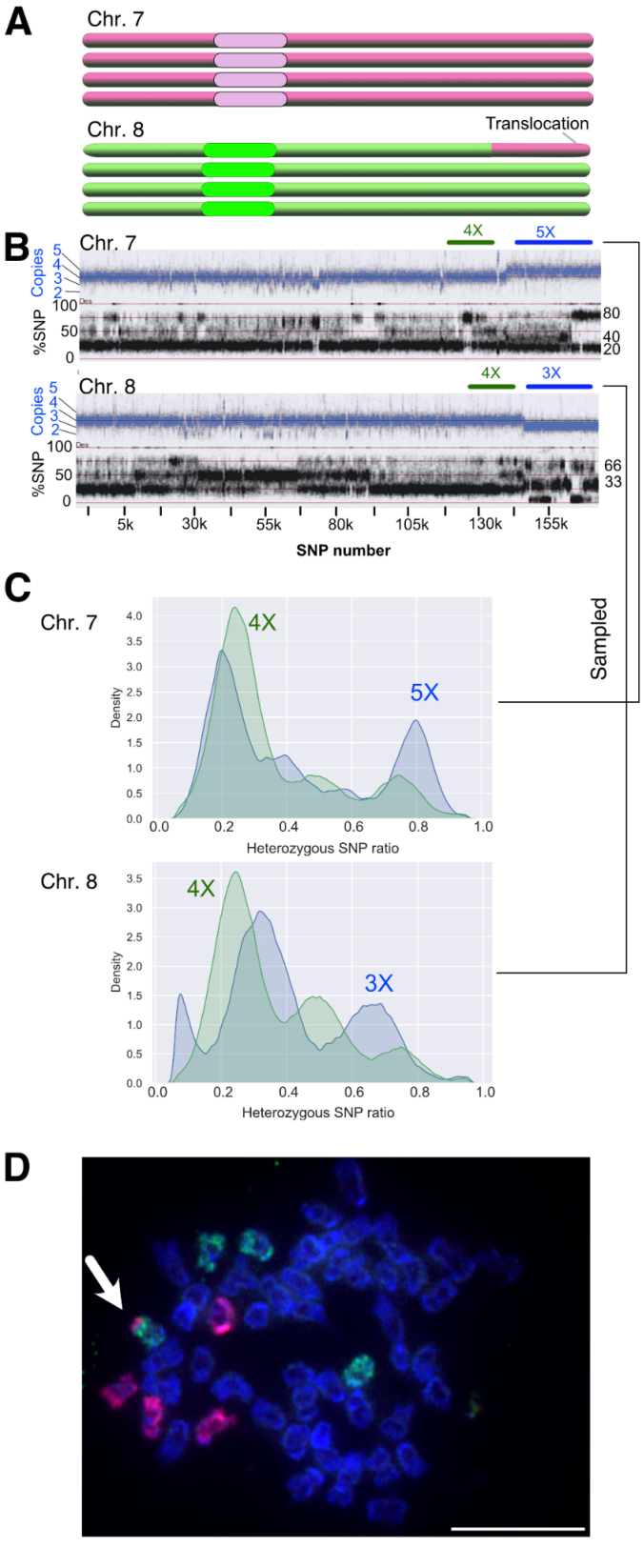

Figure 5. Molecular and cytological evidence for translocation 8-7.
The genomic status of chr. 7 and chr. 8 is demonstrated by read coverage (copy number), SNP ratio, and oligonucleotide-based fluorescent in situ hybridization painting probes (oligo-FISH). **A.** Karyotype of chr. 7 and chr. 8 in PI 310467 according to the following evidence. **B.** The blue tracks display the DNA copies at each SNP locus along the length of the shown chromosome. The multiple black tracks illustrate the allele specific read depth ratio of SNP loci. Four DNA copies yield heterozygous SNP ratios of 25-50-75%. For example, the simplex genotype *Aaaa* corresponds to 25%. Three DNA copies yield heterozygous SNP ratios of 33-66%, five copies of 20-40-60-80%. **C.** SNP ratio analysis of chr. 7 indicating 4 and 5 copies. For chr. 8, 4 and 3 copies. **D.** Oligo-FISH painting of a mitotic metaphase cell prepared from PI 310467. The arrow points to the translocation chromosome. Red: chr. 7, Green: chr. 8.

Analysis of tetraploids in the BB family of potato

To probe the robustness of the method, we analyzed the tetraploid, hybrid BB progeny. These have genomes formed by the 2x egg of PI 310467 and accidental 2N (=2x) sperms from IvP48. Their dosage states derived from the additional action of alleles, two maternal and two paternal, resulting in a more complex outcome. By Fisher Exact Test we detected comparable numbers of intrachromosomal interaction (474 in the 2x group vs 525 in the 4x group), but fewer interchromosomal interactions (764 in the 2x group vs 169 in the 4x group), as indicated by the Fisher Exact matrix. For example, the matrix no longer displayed the chr. 11-12 putative translocation visible in the 2x analysis. Tr.8-7, however, was evident (Suppl. Fig. 3). We concluded that CNV resulting from duplication or deletion are more difficult to identify in a tetraploid, but events such as Tr8-7 remain distinct.

Analysis of additional dihaploid families of potato

We asked if the method could be useful in eight comparable, but unrelated dihaploid families generated through haploid induction crosses. Seven of these dihaploid families (Amundson *et al.* 2020b) revealed the presence of translocated or misplaced heterochromatic and pericentromeric blocks, but no arm translocations (Suppl. Fig. 4, Suppl. Fig. 5). In the last dihaploid population, called LOP, an interesting arm translocation was evident that affected their tetraploid seed parent, *S. tuberosum andigena* variety Alca Tarma (Velásquez *et al.* 2007; Amundson *et al.* 2020a). Interestingly, a segment representing several Mb of euchromatin on the short arm of chr. 4 displayed a distinct dosage polymorphism that was in strong LD with the end of chr.1 (Fig. 6-A,B). Similarly to the T8-7 translocation identified in the BB population, this suggested a translocation of the euchromatic segment to the end of chr. 1, which correspondingly lost a short terminal segment. Dosage analysis in Alca Tarma demonstrated neutrality, i.e. four copies of the short arm of chr. 4. Together with the inheritance pattern observed, this suggested that the translocated chromosome T1-4 and the terminally truncated version of chr. 1 were present as a single copy in Alca Tarma (Fig. 6-C). By pooling reads from dihaploids sharing chr. 4 dosage states and rerunning the analysis with a smaller bin size, we narrowed the junction of the translocated region to a 10Kb interval between chr04.repeat.3471 and chr04.repeat.3473 (Fig. 7-A,B). This region, however, consists of N-nucleotides that could not be sequenced during the potato genome project (Fig.7-C). A model that explains the inheritance pattern and the dosage profiles of the dihaploid progeny is provided in Fig.6-C.

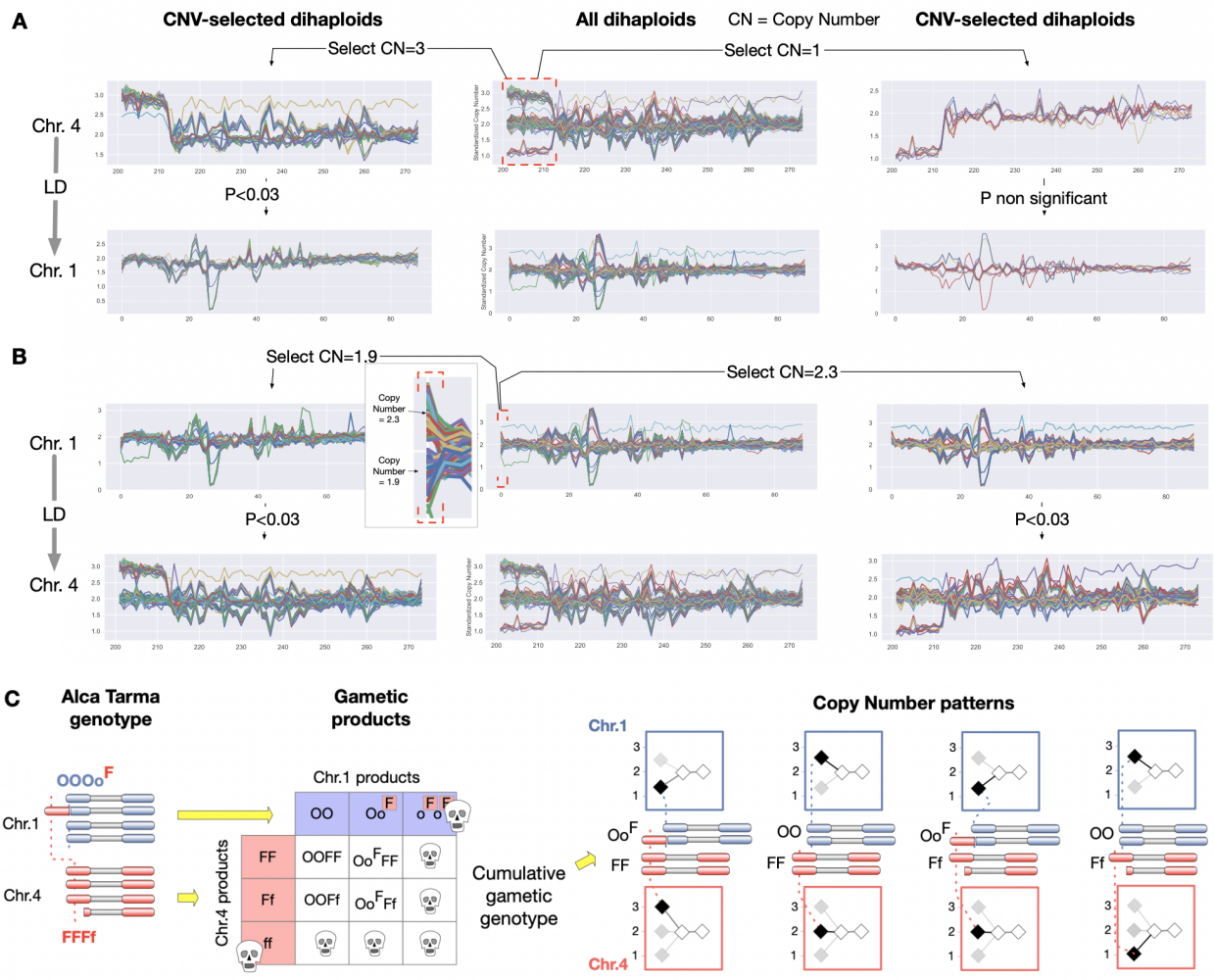

Figure 6. Linkage Disequilibrium (LD) consistent with translocation of a chr. 4 segment to chr. 1 in the LOP population.

(A-B) Each line represents the dosage profile of an individual relative to the parental control. (A). Individuals that share either high or low cluster **Copy Number** dosage state (**CN**) on the proximal arm of chromosome 4 were selected (left, right). The chromosome 1 profiles displayed by the selected individuals confirm the LD with CN=3, the duplicated state. (B). Individuals that share either high or low CN on the proximal arm of chromosome 1 are selected. The corresponding profiles for chromosome 4 confirm LD. The left arm tip of chr. 1 is enlarged to display the two dosage states. (C). Translocation model explaining two dosage states in chr.1 and three in chr. 4. A hypothetical genotype of Alca Tarma postulates that the short arm of 4 (F) translocated to the terminal 1 region (O) producing the haplotype o^F. Gametes carrying homozygous deletion or duplication are likely to be dead or impaired. The resulting dihaploids display CN patterns consistent with those observed. See Fig. 2 for an explanation of the different CN patterns.

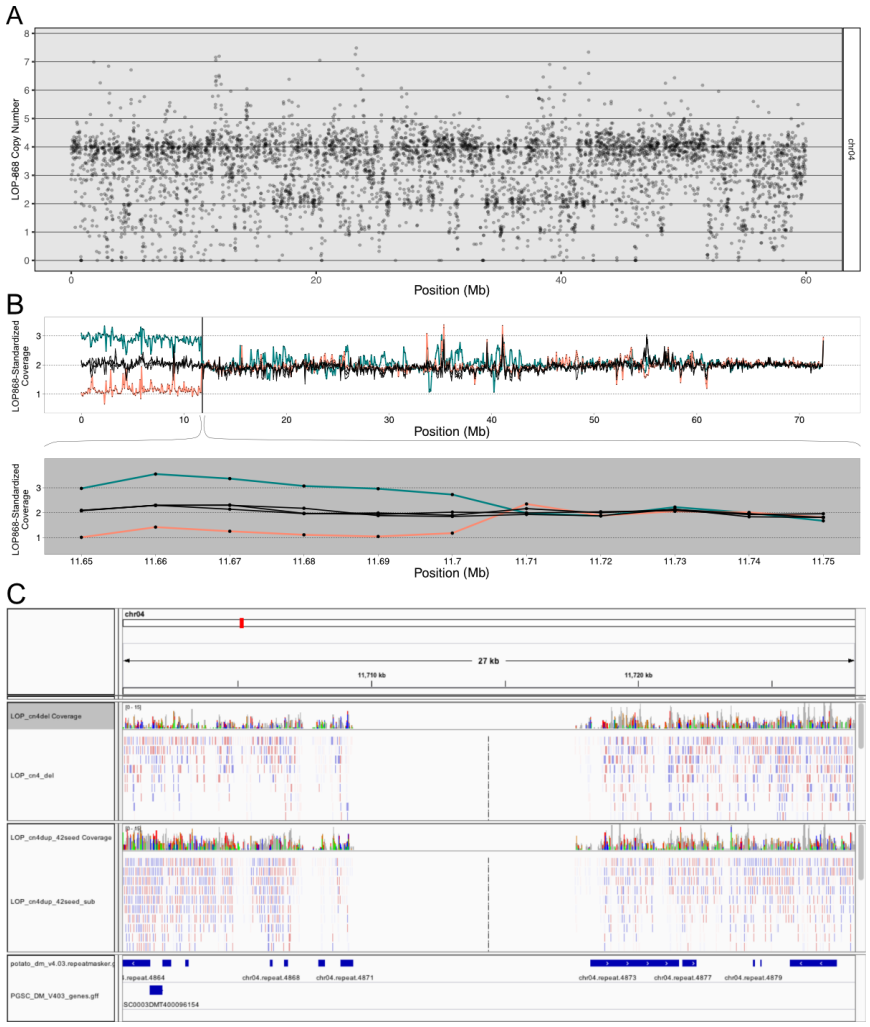

Figure 7. Breakpoint analysis of chromosome 4 short arm CNV.
A) Relative coverage in 4x Alca Tarma over contiguous non-overlapping 1Mb bins of chromosome 4. The affected euchromatic arm is dosage neutral (4 copies). B) Top track: relative mean read coverage in different pools of dihaploids derived from Alca Tarma binned in nonoverlapping 75kb bins. The lines are colored to represent duplicated (3 copies, teal, n=28 dihaploids) or deleted (pink, n=11 dihaploids) copy number states. Shown in black are three control groups, each composed of 20 randomly selected dihaploids with neither the duplicated nor deleted state. Bottom track: the zoomed-in gray region displays higher detail (10kb bins), illustrating the change from 3 or 1 to 2 copies between 11,700,000-11,710,000 bp. C) Browser view bracketing the chromosome 4 breakpoint. The top track displays reads of pooled one-copy dihaploids, the middle track the reads of pooled 3-copy dihaploids. The breakpoint is flanked by repeats 4871 and 4873, both of which are annotated as LTR/Gypsy retrotransposons.

Recurring translocations detected by LD-CNV result from genome misassembly

Comparison of LD in the nine dihaploid families highlighted frequent LD of certain heterochromatic regions across the populations (Suppl. Fig.3, 4, and 5). For example, a region in the left arm of chr. 1 was linked to the whole pericentromeric region of chr. 8. Similar translocations were evident for chr. 4 - 7 and chr. 11 - 12. Release of the *S. tuberosum* genome v.6.1 provided a test for the hypothesis of misassembly. A similarity dot matrix between these genome v.6.1 and genome v.404 (used here) displayed discordance for the translocated 1-8 and 4-7 regions (Suppl. Fig. 5) demonstrating that the detected misassembly was fixed independently in the update genome release.

Detection of related CNV patterns in an A. thaliana population

We asked if CNV in LD could be identified in an unstructured natural population of *A. thaliana* (1001 Genomes Consortium 2016). We subjected 192 randomly chosen *A. thaliana* accessions that differ in geographic origin to the CNV-LD analysis (Suppl. Table 2, Suppl. Fig. 6). Overplotting CNV states displayed mostly continuous, substoichiometric variation without the frequent and distinct dosage states found in potato. We detected significant LD between chromosomes, but these affected predominantly the pericentromeric regions and were likely determined by repetitive elements because each affected loci on multiple chromosomes.

Discussion

We developed a method that we named LD-CNV, aimed at identifying LD between copy number variable loci in the absence of genotyping information. It uses mapped reads from individuals in segregating populations. The reads are binned in genomic intervals, whose size depends on sequence coverage, but typically ranges from 0.1 to 1Mb. Read counts are normalized to the value of a reference, for example the parent, scaling the mean to overall ploidy. We identify dosage polymorphic bins by detecting variation and clustered dosage values among the tested individuals (Fig.1,2). We then test for association between dosage states of different variable bins using Fisher Exact test (Fig. 2,3). An alternative approach is to simply measure correlation using the input dosage values or the peak-centered processed values. Regardless of the statistical tool chosen, the method is simple, aiming to identify discrepancies from available genomic models. A related method, CNVmap, differs from ours by leveraging heterozygous SNP as a proxy for duplicated loci and mapping them in segregating populations (Falque *et al.* 2019). Therefore, it detects small scale duplications, but only when their sequence is divergent. The independence of LD-CNV from genotyping makes it applicable in a fully homozygous system or in any system lacking genotyping information.

We provide the software as annotated Jupyter Notebooks. These are Python-based data analysis tools that facilitate pipeline journaling, annotation, and modification for flexible analysis

(Perkel 2018). In addition, plotting and display of data series from the data frames is accessible at any step of the execution (Waskom; Hunter 2007). Software dependencies can be easily installed and managed via Anaconda ("Anaconda"). Complexity and computing power of these tools are scalable, but for most analyses, such as those described here, consumer hardware is sufficient. These features should make the tool both readily usable and modifiable for ad hoc applications.

We originally developed this method to identify epistatic relationships between SV loci in potato, assuming that they would result in LD. We found, however, that the strongest signals were the result of physical LD. In our potato dihaploid progeny populations, LD-CNV analysis identified two heterochromatic blocks that were misassembled in the original reference genome and corrected in the latest one. Providing further validation, in two tetraploid seed mother accessions out of the nine tested in this analysis, we found convincing evidence of chromosomal translocations involving euchromatic arms. We detected LD between the right arms of chr. 7 and chr. 8 in the BB population (seed parent var. PI 310467), and the left arms of chr. 1 and chr. 4 in the LOP population (seed parent var. Alca Tarma). This information was combined with dosage analysis to generate translocation models. In the BB seed parent PI 310467, 5 and 3 copies, respectively, of the terminal regions of chr. 7 and chr. 8, suggested that the terminal right arm of chr. 7 translocated to chr. 8 with concurrent loss of the terminal region of chr. 8 (Fig. 6-A,B). The BB population included a tetraploid set, which enabled testing the method in a genomic scenario more challenging than diploidy. In the tetraploids, haplotypes are contributed by the tetraploid seed mother and the diploid pollen parent. Nonetheless, detection of the 8-7 translocation was still possible. The predicted rearrangement was confirmed by oligo-FISH analysis (Han *et al.* 2015; Braz *et al.* 2018) in the BB population parent. A second translocation was detected in Alca Tarma, the seed parent of LOP. In this clone, chr. 1 and chr. 4 appear copy-number neutral. This information, together with the profiles of the dihaploid progeny, supports a model in which the terminal region of chr. 4 translocated near to the end of chr. 1 (Fig. 6-C).

We wondered whether this new tool could inform us about structural variation in natural populations as well, and tested a set of 192 *A. thaliana* accessions. Comparison of the results obtained with pedigree families to this natural population shows the effect of an important feature: sibs in segregating populations form distinct dosage clusters when inheriting CNV haplotypes that are heterozygous in the parent. Large haplotypes are conserved in most individuals because recombination is rare. Large genomic bins in natural populations, however, vary continuously because of the independent behavior of multiple DNA regions and elements, hindering formation of distinct clusters. The copy number variation observed in the *A. thaliana* population corresponds most likely to repeated regions, while those observed in the potato families includes single copy sequences. The analysis should work in natural populations if the bin unit examined is very small, such as gene-size. On that scale, presence-absence of a DNA segment should cluster nicely on two dosage states. That level of granularity would require more computing power than provided by consumer hardware. If one is interested in new variation,

however, LD would likely be confined to only a few bins and easily analyzed.

In conclusion, the method enables exploration of sequence datasets from segregating families in species with a reference genome to identify relationships among SV loci. Mb scale variation can be detected with as little as 0.2X coverage since one can expand bin size to increase the number of reads to a threshold of statistical confidence. Low-pass, whole-genome sequencing is a convenient approach toward genotyping that is becoming rapidly more affordable (DePristo *et al.* 2011). Once sequence reads have been mapped, the method is easily implemented without the need to identify a set of informative SNP. Knowledge of translocations, whether real or caused by genome mis-assembly, is critical to the use of a genetic population for genetic studies and for breeding because of the dramatic effect they can have on outcome and interpretation.

Methods

Dosage Analysis

Single end reads were aligned to the DM1-3 4.04 reference *Solanum tuberosum* genome with BWA-mem (Li 2013) and only reads with mapping quality ≥Q10 were retained. Standardized coverage values were derived by taking the fraction of mapped reads that aligned to a bin of interest for that sample, normalizing it to the corresponding fraction from the same interval in in the parent of the population, if available, or the mean of the population, and multiplying the resulting value by 2 to indicate the expected diploid state, as previously described (Henry *et al.* 2015). To mitigate mapping bias due to read type and length, paired end reads from LOP-868 were hard trimmed to 50 nt and only forward mates were used for analysis. Read depth is calculated for fixed-size non-overlapping windows, set to 250kb or 1Mb in this study. Whole chromosome aneuploids are identified as previously described (Amundson *et al.* 2020a) and withheld from analysis prior to LD matrix construction.

Linkage Disequilibrium

The analysis and figure generating software is available at https://github.com/lcomai/cnv_mapping. Fisher's Exact test was carried out between pairs of dosage states derived from 1Mb bins to assess linkage disequilibrium between bins. For example, assume that both Bin1 and Bin100 have three dosage states: copy number 1, 2 and 3. To test if Bin1 correlated to Bin100, the following four dihaploid sets were compared in a 2x2 contingency table: *observed in Bin1-CN1 : observed not in Bin1-CN1, expected in Bin1-CN1 : expected not in Bin1-CN1*, where the expectation was derived from the assumption of complete independence. Self-comparison and reciprocal comparisons were removed, and the remaining comparisons controlled at FDR = 0.05. Chromosomal bins that were engaged in at least one statistically significant correlation after these corrections were deemed in LD.

Alternative to Fisher Exact analysis of copy number dosage states, one can derive and plot a heatmap of correlation coefficients such as Pearson's R as demonstrated in the Github

notebooks (See above) and in Suppl. Fig. 3 and 4. Gating the resulting matrix to display only the strongly correlated values helps in the analysis (Suppl. Fig. 3 and 4). Measuring correlation with a utility such as *DataFrame.corr()* (Pandas) or *scipy.stats.pearsonr()* avoids the bin-by-bin Fisher Exact analysis, which becomes computationally intensive with increasing numbers of CNV bins. Nonetheless, we found the Fisher Exact approach manageable and clearer in its output. Categorization in peaks (dosage clusters) helped the subsequent analysis of candidate regions.

Chromosome spread preparation

Potatoes were planted from culture tubes into a greenhouse planting mix and allowed to grow for 3-5 days. The root tips were collected and treated with iced water for 24h. Then, the root tips were fixed directly into Carnoy's solution (3 ethanol: 1 acetic acid) and stored at -20°C until use. The root tips were squashed on the microscope slide with the same fixative solution after digestion with 2% cellulose (Sigma, USA) and 1% pectolyase (Sigma, USA) at 37℃ for 2h.

Oligo-FISH painting

We used oligonucleotide-based FISH probes (Oligo-FISH) (Han et al. 2015) to specifically paint the chromosomes 7 and 8 of potato. Probe labeling and FISH were performed following published protocols (Braz *et al.* 2018, 2020). Biotin and digoxygenin-labeled probes were detected by anti-biotin fluorescein (Vector Laboratories, Burlingame, CA, USA) and anti-digoxygenin rhodamine (Roche Diagnostics, Indianapolis, IN, USA), respectively. Chromosomes were counterstained with 4,6-diamidino-2-phenylindole in VectaShield antifade solution (Vector Laboratories). The chromosome spreads were imaged using a QImaging Retiga EXi Fast 1394 CCD camera (Teledyne Photometrics, Tucson, AZ, USA) attached to an Olympus BX51 epifluorescence microscope. Images were processed with META IMAGING SERIES 7.5 software and their final contrast was processed using Adobe PHOTOSHOP software (Adobe, San Jose, CA, USA).

Data availability

Sequence data have been obtained from or deposited in the National Center for Biotechnology Information Sequence Read Archive with the following Bio-Project identifier: for the LOP dihaploids, PRJNA408137; BB, reads submission is pending; sequence reads data for the dihaploids of WA077, lr00014, lr00022, lr00026, 93003, C91640, C93154, are at NCBI Bioproject PRJNA699631. The raw and standardized genomic dosage values for the BB dihaploids are available at DryadData.com https://doi.org/10.25338/B88D2V. The arabidopsis sequence listed in Suppl. Table 2 was obtained from PRJNA273563 "1001 Genomes: A Catalog of Arabidopsis thaliana Genetic Variation".

Acknowledgments

This work was supported by: the National Science Foundation Plant Genome Integrative Organismal Systems (IOS) Grants 1444612 (Rapid and Targeted Introgression of Traits via Genome Elimination) and 1956429 (RESEARCH-PGR: Variants and Recombinants without Meiosis) to L.C. and I.M.H; a grant from the Innovative Genome Institute at UC Berkeley to LC, and the United States - Israel Binational Agricultural Research and Development Funds IS-5038-17C and IS-5317-20C to J.J.

Author contributions

L.C. designed experiments with input from K.R.A. and I.M.H.. L.C., K.R.A., and B.O performed genomic experiments. XZ, GTB, and JJ performed cytological experiments. L.C. analyzed data and wrote the manuscript with input from all authors.

Supplemental Figures and Tables

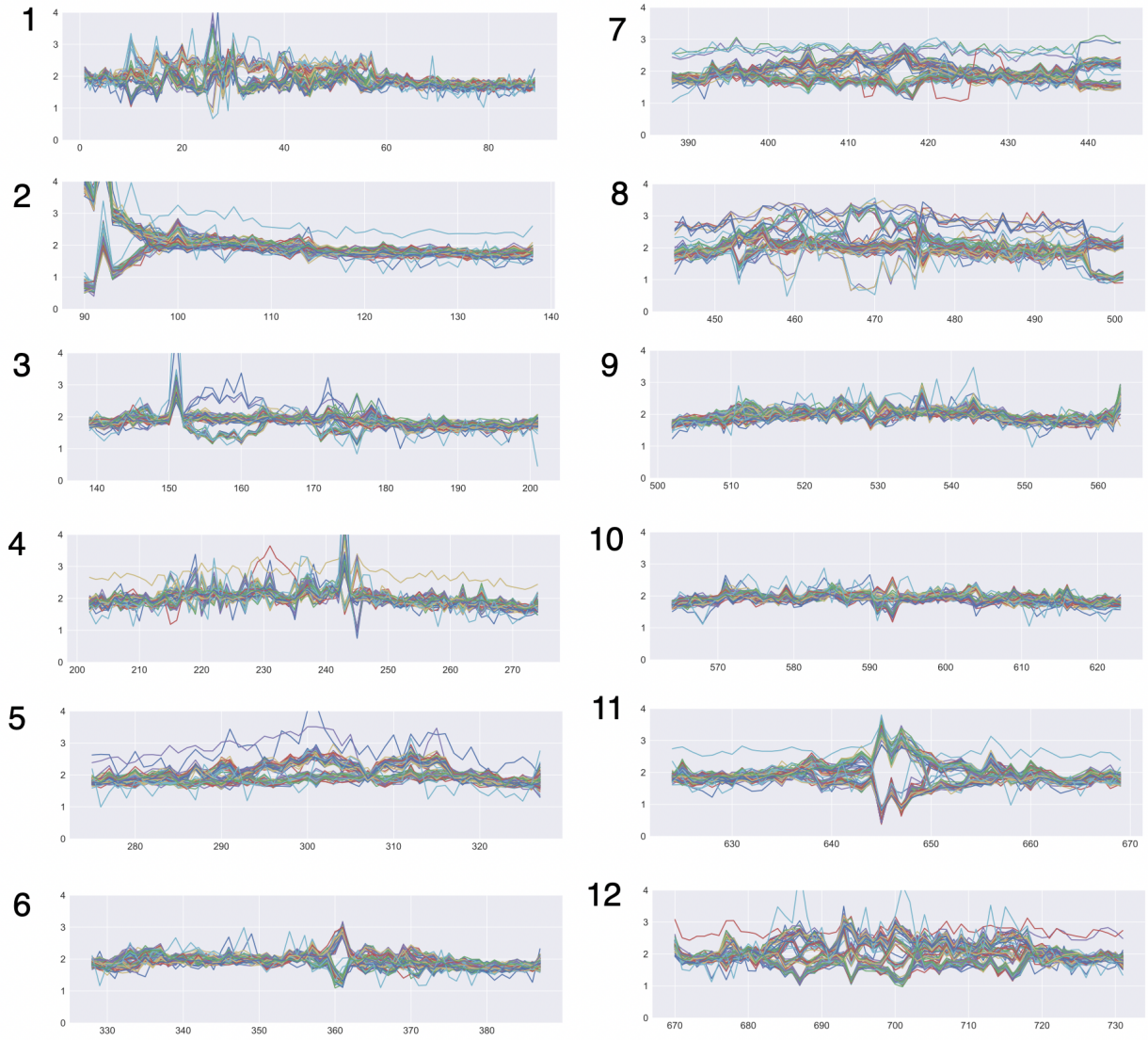

Supplemental Fig. 1. CNV patterns in BB, the dihaploid population of potato cv. PI 310467. The dosage tracks of 84 2x individuals produced by crossing cv. PI 310467 to haploid inducer IvP48.

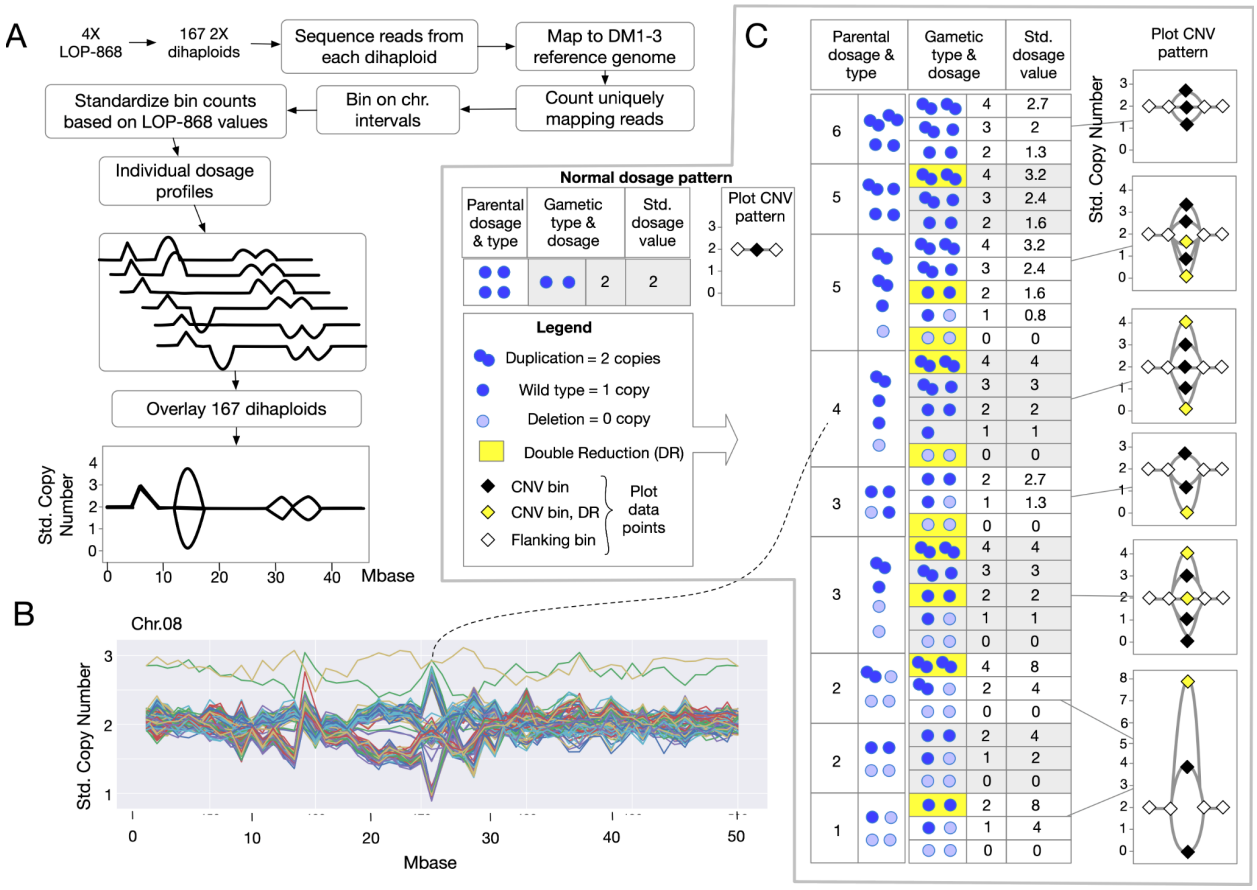

Supplemental Fig. 2. Analysis of CNV.

A. Overview of method to produce the dosage plot using a dihaploid family produced from an autotetraploid parent (LOP868 is the CIP accession name for Alca Tarma, the parent of the LOP population). B. Example of dosage plot resulting from the plotting of dihaploid profiles. Each color represents an individual. The two outliers are trisomics for chr. 8. C. Dosage variation in the autotetraploid parent and resulting segregation patterns in the dihaploids, which represent the maternal gametes. The relative dosage is calculated from the formula: $(CN^{2x}/CN^{4x}) * 4$, where *CN* is the copy number and *nx* the ploidy of the individual.

Dark blue: present allele. Light blue: absent allele (deletion). Overlapping circles represent a duplicated allele inherited as a unit. Yellow cells represent gametes formed by double reduction. Double reduction occurs at low frequency and is dependent on the recombination frequency between the locus of interest and the centromere.

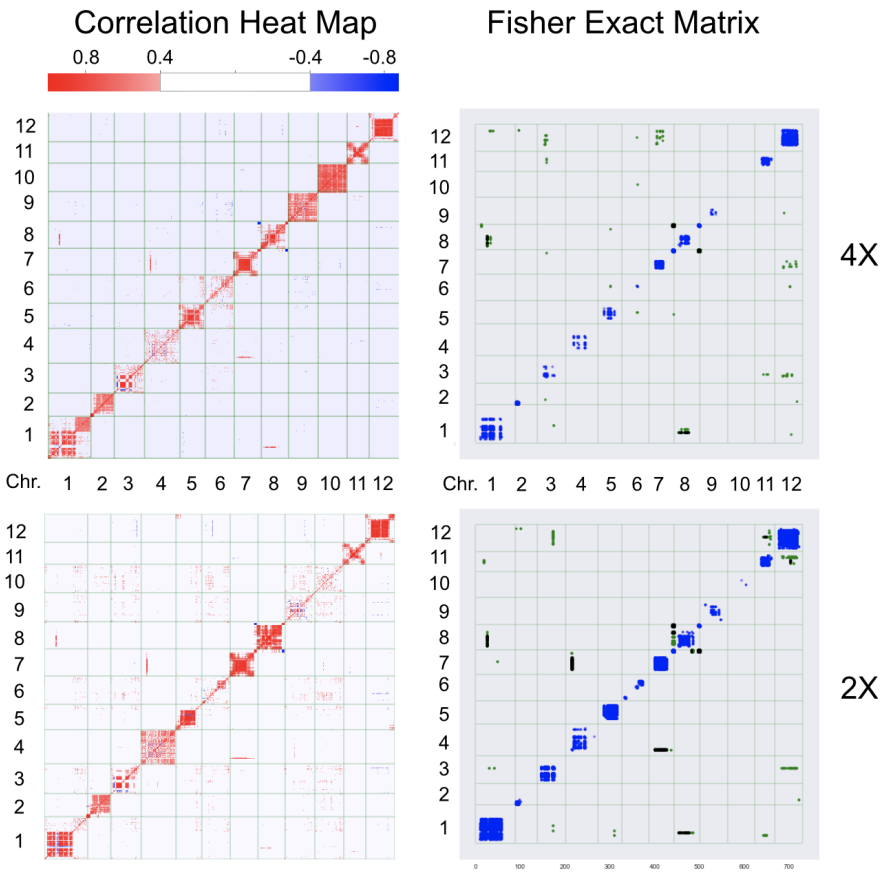

Supplemental Fig. 3. Effect of ploidy and statistical method on LD analysis.
4X analyses used the tetraploids of the BB population. 2X analyses used the diploids. The use of the Pearson's Correlation matrix and the implementation of the Fisher Exact matrix are presented in Methods and are available at https://github.com/lcomai/cnv_mapping.

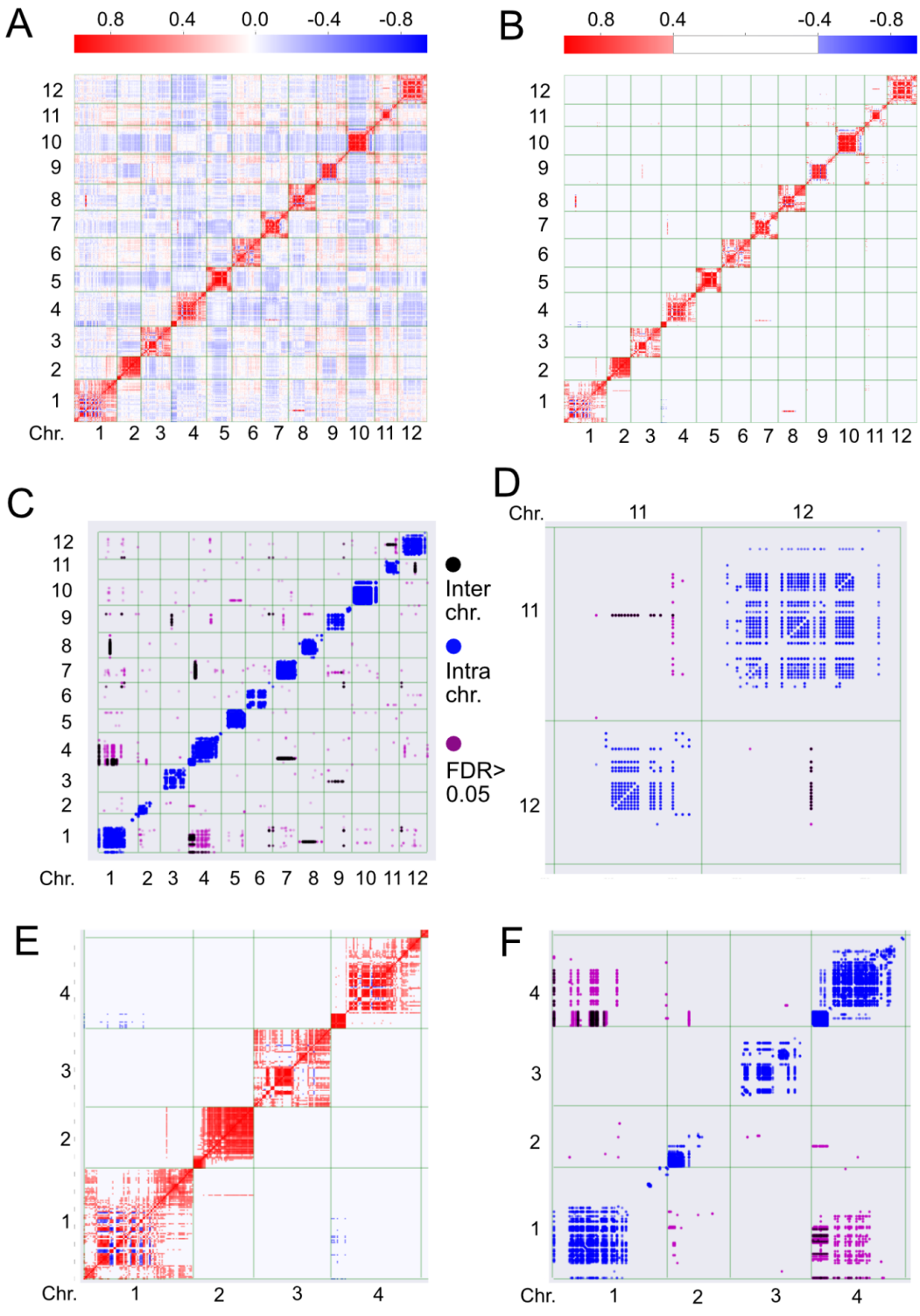

Supplemental Fig. 4. Analysis of the LOP dihaploid family and comparison of Pearson's Correlation and Fisher Exact test for detection of correlated CNV sites.

A. Raw correlation heatmap is less specific and more difficult to interpret than the Fisher Exact matrix. B. Improved heatmap display by filtering low correlation signals. **C.** Clear demarcation of candidate correlated regions by cluster analysis and Fisher Exact test. A major signal is visible for chromosome 1 and 4. D. Fisher Exact identifies candidate regions in chr. 11 and 12. This appears to be the same signal displayed by the BB population, suggesting that two different cultivated potatoes share polymorphism. E, F. Side by side comparison of translocation signals in filtered correlation and Fishes Exact matrices.

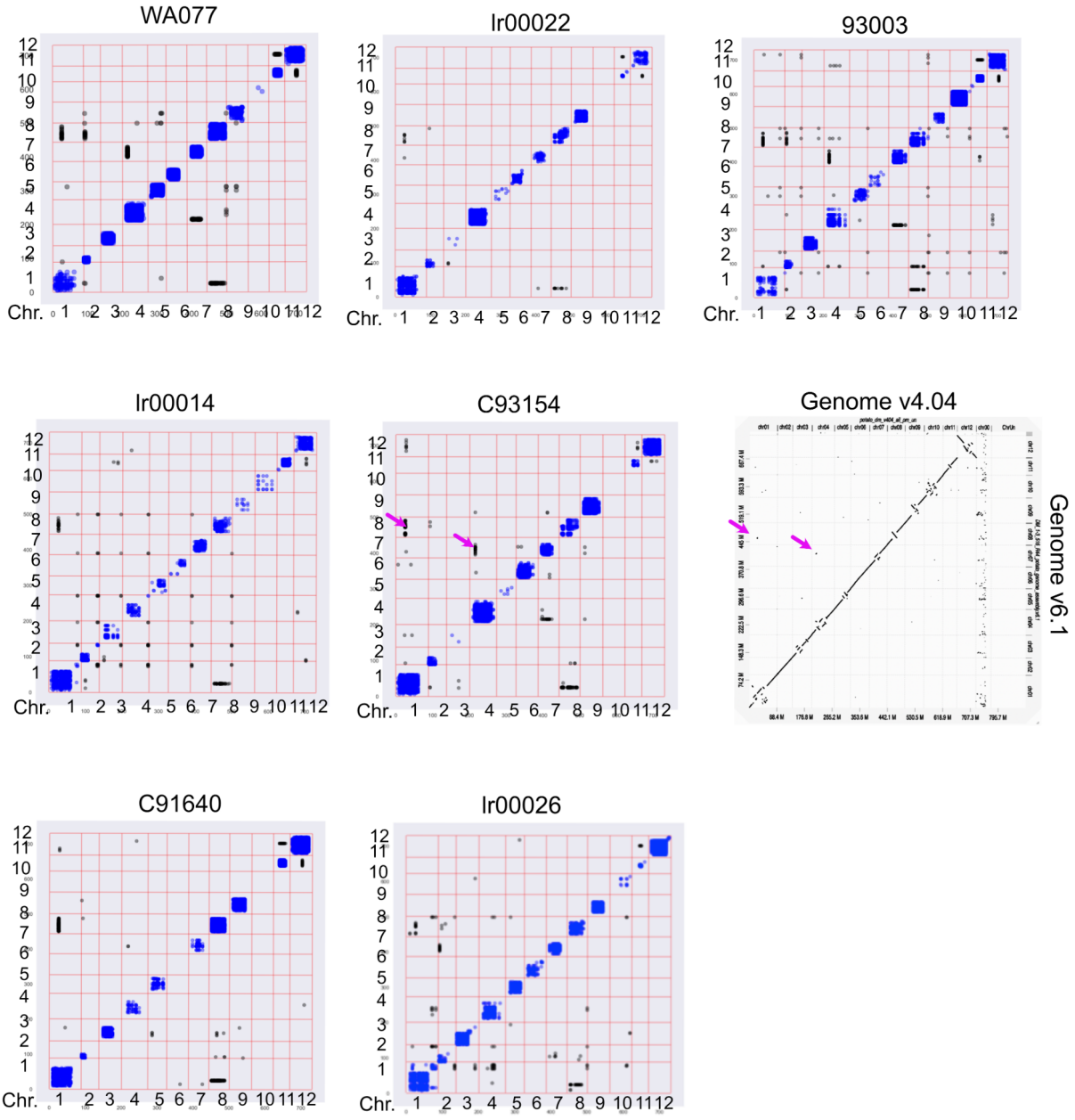

Supplemental Fig. 5. Fisher Exact LD matrices from seven potato populations.
The name of each dihaploid family seed parent is shown on top of each matrix. Blue: intrachromosomal LD. Black: interchromosomal LD. In all cases, the interchromosomal signals are consistent with pericentromeric translocation or misassembly during construction of the reference genome. The 8th matrix is a dot matrix comparison (Cabanettes and Klopp 2018) of the genome assembly version used in this work (4.04) to a more recent one (6.1). The magenta

arrows point to regions in chromosome 8 vs 1 and 7 vs 4 that were misassembled in 4.04 and appear "translocated" in multiple population analyses. The absence of the signal in some populations could be due to the lack of segregating CNV in those regions.

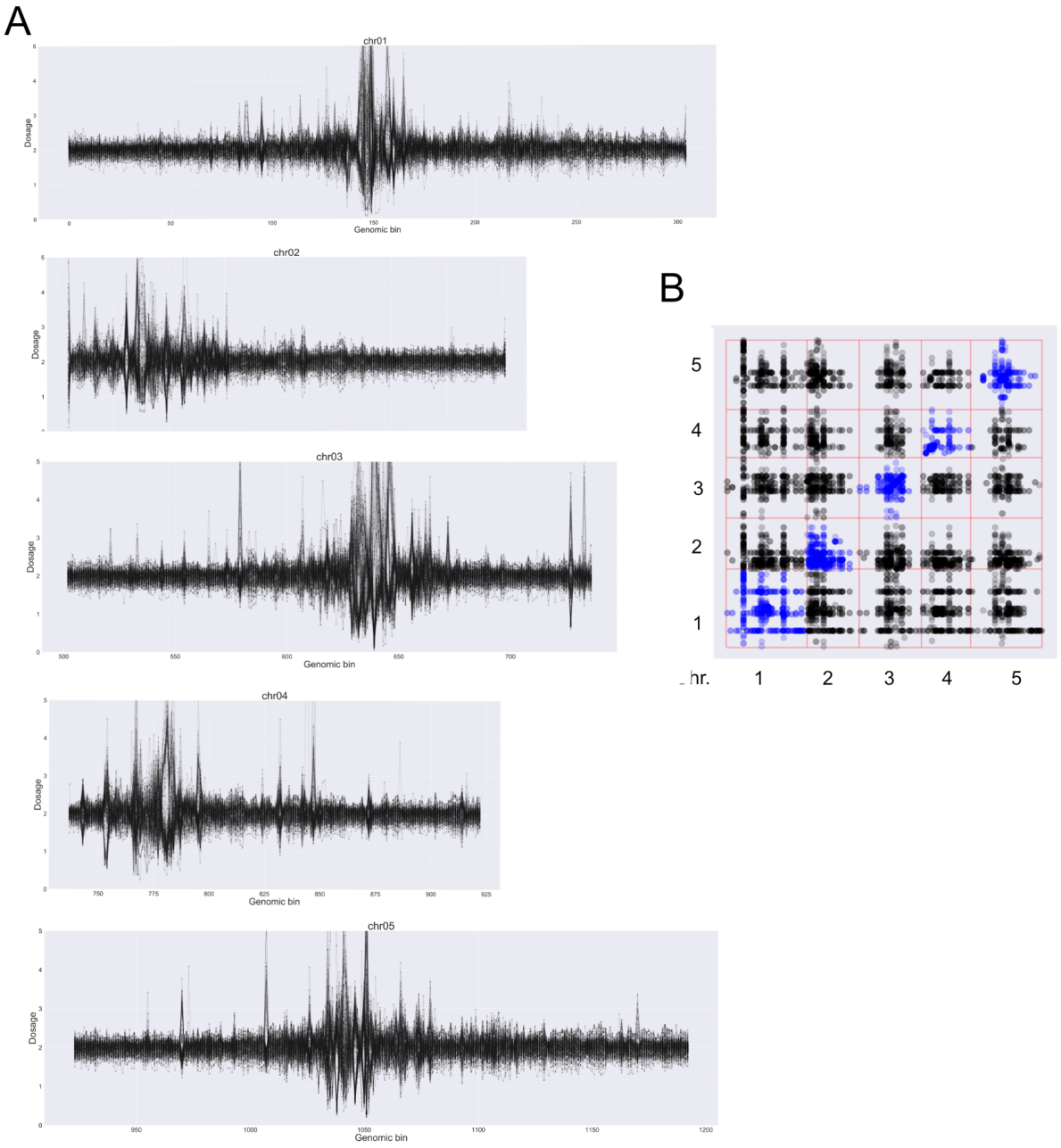

Supplemental Fig. 6. Analysis of CNV in Arabidopsis natural accessions.

A. Chromosomal dosage profiles (chr. 1 to chr. 5, top to bottom) for the 192 *A. thaliana* accessions in Supplemental Table 1. B. Linkage Disequilibrium Matrix of Fisher Exact dosage correlation analysis for bins with FDR = 0.05 and for which the dosage difference between peaks is at least 1. Black: interchromosomal, blue: intrachromosomal. The interchromosomal signals demonstrate LD common to most pericentromeric regions and therefore likely caused by repeats.

Supplemental Table 1. List of potato accessions and sequencing library deposit

Population Name	Tetraploid parent	Haploid inducer	Project number in NCBI read sequence database
LOP	Alca Tarma, a.k.a LOP 868	PL-4, IvP-101	PRJNA408137
BB	PI 310467, cv. Desiree in germplasm collection	IvP-48	Raw sequence in progress. Binned dosage values are at https://doi.org/10.25338/B88D2V
WA077	WA077 (CIP397077.16 or cv. Alliance/Sarnav)	PL-4, IvP-101	PRJNA699631
lr00014	lr00014 (CIP300056.33)		
lr00022	lr00022 (CIP300072.1)		
lr00026	lr00026 (CIP300093.14)		
93003	93003 (CIP390637.1)		
C91640	C91640 (CIP388615.22)		
C93154	C93154 (CIP392820.1 or cv. BARI Alu-73)		

Supplemental Table 2. List of Arabidopsis accessions, SRA number and sequencing library characteristics

Accession + SRR (run name in SRA db at NCBI PRJNA273563)	**Reads**	**Reads/MB**
admixed-GMI-10_SRR1946059	59916068	500686.84
admixed-GMI-11_SRR1945728	24022752	200745.41
admixed-GMI-12_SRR1945997	29659042	247844.9
admixed-GMI-13_SRR1946061	33793413	282393.65
admixed-GMI-14_SRR1946077	34644790	289508.16
admixed-GMI-15_SRR1945983	19010462	158860.36
admixed-GMI-1_SRR1945626	19800036	165458.41
admixed-GMI-2_SRR1946071	28704624	239869.34
admixed-GMI-3_SRR1945491	40568849	339012.38
admixed-GMI-4_SRR1946022	36515150	305137.77
admixed-GMI-5_SRR1945490	16039451	134033.2
admixed-GMI-6_SRR1945623	19421444	162294.72
admixed-GMI-7_SRR1946069	21392755	178767.92
admixed-GMI-8_SRR1946070	30120943	251704.77
admixed-GMI-9_SRR1945638	32841499	274439.01
admixed-Monsanto-10_SRR1945537	9055319	75670.5
admixed-Monsanto-11_SRR1946183	16810601	140477.29
admixed-Monsanto-12_SRR1946126	17673420	147687.41
admixed-Monsanto-13_SRR1946184	21228594	177396.12
admixed-Monsanto-14_SRR1946471	13767340	115046.37
admixed-Monsanto-15_SRR1946400	12540265	104792.35
admixed-Monsanto-1_SRR1945940	10699758	89412.21
admixed-Monsanto-2_SRR1945519	15019671	125511.43
admixed-Monsanto-3_SRR1946108	17166146	143448.39

admixed-Monsanto-4_SRR1946149	15577834	130175.71
admixed-Monsanto-5_SRR1946418	5990357	50058.24
admixed-Monsanto-6_SRR1946135	17295878	144532.49
admixed-Monsanto-7_SRR1945556	9700463	81061.63
admixed-Monsanto-8_SRR1946479	17924451	149785.14
admixed-Monsanto-9_SRR1946438	13674684	114272.09
asia-GMI-1_SRR1946559	28507994	238226.21
asia-GMI-2_SRR1946560	55378823	462771.49
asia-GMI-3_SRR1946561	41916903	350277.36
asia-GMI-4_SRR1946558	25864327	216134.48
asia-GMI-5_SRR1946555	27246541	227684.91
asia-GMI-6_SRR1946566	35257170	294625.49
asia-GMI-7_SRR1946557	24278378	202881.54
asia-GMI-8_SRR1946565	41394961	345915.76
asia-GMI-9_SRR1946556	27748807	231882.08
asia-Monsanto-10_SRR1946049	30564177	255408.64
asia-Monsanto-11_SRR1946212	12655516	105755.44
asia-Monsanto-12_SRR1946225	12970324	108386.13
asia-Monsanto-13_SRR1946218	9342590	78071.08
asia-Monsanto-14_SRR1946312	9520464	79557.47
asia-Monsanto-15_SRR1946203	13293030	111082.81
asia-Monsanto-1_SRR1946229	11167396	93320.01
asia-Monsanto-2_SRR1946214	9013359	75319.87
asia-Monsanto-3_SRR1946219	8855134	73997.66
asia-Monsanto-4_SRR1946224	9790332	81812.62
asia-Monsanto-5_SRR1946199	12179493	101777.57
asia-Monsanto-6_SRR1946201	11459167	95758.19
asia-Monsanto-7_SRR1946221	12692203	106062.02

asia-Monsanto-8_SRR1946050	23325425	194918.22
asia-Monsanto-9_SRR1946216	11455734	95729.5
central_europe-GMI-1_SRR1946008	19335113	161573.3
central_europe-GMI-2_SRR1946569	40264985	336473.15
central_europe-GMI-3_SRR1946563	69280709	578942.19
central_europe-GMI-4_SRR1946562	63443436	530163.19
central_europe-GMI-5_SRR1945724	20054005	167580.7
central_europe-GMI-6_SRR1946564	68211731	570009.3
central_europe-GMI-7_SRR1946568	36714388	306802.69
central_europe-GMI-8_SRR1946567	44576218	372499.84
central_europe-Monsanto-10_SRR1946230	12765831	106677.29
central_europe-Monsanto-11_SRR1946268	19014619	158895.1
central_europe-Monsanto-12_SRR1945887	11104130	92791.33
central_europe-Monsanto-13_SRR1946343	20579298	171970.29
central_europe-Monsanto-14_SRR1946465	11770417	98359.14
central_europe-Monsanto-15_SRR1946247	10763715	89946.66
central_europe-Monsanto-1_SRR1946249	9821512	82073.17
central_europe-Monsanto-2_SRR1946252	13265534	110853.04
central_europe-Monsanto-3_SRR1945443	16016473	133841.18
central_europe-Monsanto-4_SRR1946263	15117094	126325.55
central_europe-Monsanto-5_SRR1946254	14385342	120210.68
central_europe-Monsanto-6_SRR1946272	11963830	99975.39
central_europe-Monsanto-7_SRR1946266	20927166	174877.24
central_europe-Monsanto-8_SRR1946363	22051503	184272.73
central_europe-Monsanto-9_SRR1946369	21010693	175575.23
germany-GMI-10_SRR1946094	64112581	535754.88
germany-GMI-11_SRR1946103	20588686	172048.74
germany-GMI-12_SRR1945757	14245174	119039.37

germany-GMI-1_SRR1946009	17541288	146583.25
germany-GMI-2_SRR1945729	79383009	663361.76
germany-GMI-3_SRR1945696	25408557	212325.85
germany-GMI-4_SRR1945793	28859058	241159.86
germany-GMI-5_SRR1945727	10380604	86745.21
germany-GMI-6_SRR1945726	23114360	193154.46
germany-GMI-7_SRR1945943	17913268	149691.69
germany-GMI-8_SRR1945944	10227695	85467.43
germany-GMI-9_SRR1945730	57664135	481868.63
germany-Monsanto-10_SRR1945873	9570405	79974.81
germany-Monsanto-11_SRR1945468	15082766	126038.69
germany-Monsanto-12_SRR1945575	17094637	142850.83
germany-Monsanto-13_SRR1945960	8887338	74266.78
germany-Monsanto-14_SRR1945507	23900073	199720.25
germany-Monsanto-15_SRR1945513	15828270	132268.47
germany-Monsanto-1_SRR1945515	14431836	120599.21
germany-Monsanto-2_SRR1945474	10955767	91551.54
germany-Monsanto-3_SRR1945473	22297592	186329.17
germany-Monsanto-4_SRR1945961	9722146	81242.82
germany-Monsanto-5_SRR1945538	14253405	119108.16
germany-Monsanto-6_SRR1946469	15668800	130935.86
germany-Monsanto-7_SRR1945583	22458306	187672.17
germany-Monsanto-8_SRR1945531	19783897	165323.55
germany-Monsanto-9_SRR1945554	9266572	77435.83
italy_balkan_caucasus-Monsanto-10_SRR1946282	7402735	61860.74
italy_balkan_caucasus-Monsanto-11_SRR1946297	19763662	165154.45
italy_balkan_caucasus-Monsanto-12_SRR1946240	9828609	82132.48
italy_balkan_caucasus-Monsanto-13_SRR1946032	18279195	152749.55

italy_balkan_caucasus-Monsanto-14_SRR1946321	10435351	87202.7
italy_balkan_caucasus-Monsanto-15_SRR1946323	21265077	177700.98
italy_balkan_caucasus-Monsanto-1_SRR1946288	11969392	100021.87
italy_balkan_caucasus-Monsanto-2_SRR1946046	16701439	139565.08
italy_balkan_caucasus-Monsanto-3_SRR1946301	9280705	77553.94
italy_balkan_caucasus-Monsanto-4_SRR1946023	13498714	112801.6
italy_balkan_caucasus-Monsanto-5_SRR1946291	11484184	95967.24
italy_balkan_caucasus-Monsanto-6_SRR1946036	31954866	267029.89
italy_balkan_caucasus-Monsanto-7_SRR1946292	14538360	121489.37
italy_balkan_caucasus-Monsanto-8_SRR1946025	19477965	162767.04
italy_balkan_caucasus-Monsanto-9_SRR1946295	11013689	92035.57
north_sweden-GMI-10_SRR1945690	35646246	297876.8
north_sweden-GMI-11_SRR1945716	13063824	109167.46
north_sweden-GMI-12_SRR1946090	37244466	311232.27
north_sweden-GMI-13_SRR1946007	18173335	151864.93
north_sweden-GMI-14_SRR1945632	21309495	178072.16
north_sweden-GMI-15_SRR1945630	26677852	222932.68
north_sweden-GMI-1_SRR1945604	16929373	141469.8
north_sweden-GMI-2_SRR1945715	16638157	139036.26
north_sweden-GMI-3_SRR1945697	34935477	291937.28
north_sweden-GMI-4_SRR1945694	26013634	217382.16
north_sweden-GMI-5_SRR1945607	38118179	318533.43
north_sweden-GMI-6_SRR1945605	58226536	486568.32
north_sweden-GMI-7_SRR1945711	36444439	304546.87
north_sweden-GMI-8_SRR1945691	24890971	208000.66
north_sweden-GMI-9_SRR1946064	17125390	143107.81
relict-Monsanto-10_SRR1946427	11670262	97522.2
relict-Monsanto-11_SRR1946195	11254133	94044.83

relict-Monsanto-12_SRR1946393	13088955	109377.46
relict-Monsanto-13_SRR1946152	18967479	158501.18
relict-Monsanto-14_SRR1946443	16060723	134210.95
relict-Monsanto-15_SRR1946398	17903397	149609.21
relict-Monsanto-1_SRR1946147	20211669	168898.21
relict-Monsanto-2_SRR1946143	14356021	119965.66
relict-Monsanto-3_SRR1946168	16425998	137263.36
relict-Monsanto-4_SRR1946140	17347996	144968.01
relict-Monsanto-5_SRR1946192	20661996	172661.36
relict-Monsanto-6_SRR1946190	13805415	115364.54
relict-Monsanto-7_SRR1946436	18121950	151435.54
relict-Monsanto-8_SRR1946132	16429270	137290.71
relict-Monsanto-9_SRR1946458	9246205	77265.64
south_sweden-GMI-10_SRR1946101	40376693	337406.64
south_sweden-GMI-11_SRR1945636	15148525	126588.2
south_sweden-GMI-12_SRR1945648	39477578	329893.21
south_sweden-GMI-13_SRR1945698	19662788	164311.5
south_sweden-GMI-14_SRR1946100	38782621	324085.82
south_sweden-GMI-15_SRR1945660	27492214	229737.87
south_sweden-GMI-1_SRR1945633	35549994	297072.47
south_sweden-GMI-2_SRR1945637	38539759	322056.35
south_sweden-GMI-3_SRR1945683	35359557	295481.09
south_sweden-GMI-4_SRR1945996	28208636	235724.63
south_sweden-GMI-5_SRR1945964	15576292	130162.82
south_sweden-GMI-6_SRR1945477	19110039	159692.47
south_sweden-GMI-7_SRR1945707	30146186	251915.71
south_sweden-GMI-8_SRR1946087	39000378	325905.5
south_sweden-GMI-9_SRR1946092	23810485	198971.61

south_sweden-Monsanto-1_SRR1945906	11470851	95855.83
spain-Monsanto-10_SRR1946155	15160643	126689.46
spain-Monsanto-11_SRR1946151	13526890	113037.05
spain-Monsanto-12_SRR1946402	14183058	118520.3
spain-Monsanto-13_SRR1946435	16866069	140940.8
spain-Monsanto-14_SRR1946412	12964849	108340.38
spain-Monsanto-15_SRR1946451	16753696	140001.76
spain-Monsanto-1_SRR1946437	13150132	109888.69
spain-Monsanto-2_SRR1946381	12589966	105207.68
spain-Monsanto-3_SRR1946404	8464114	70730.12
spain-Monsanto-4_SRR1946453	15113990	126299.61
spain-Monsanto-5_SRR1946426	14461779	120849.43
spain-Monsanto-6_SRR1946154	17281639	144413.5
spain-Monsanto-7_SRR1946133	20868196	174384.46
spain-Monsanto-8_SRR1946167	18623040	155622.88
spain-Monsanto-9_SRR1946454	18006844	150473.66
western_europe-GMI-1_SRR1945657	26646916	222674.16
western_europe-Monsanto-10_SRR1946389	13761980	115001.58
western_europe-Monsanto-11_SRR1945553	7896785	65989.25
western_europe-Monsanto-12_SRR1946480	11433818	95546.36
western_europe-Monsanto-13_SRR1945456	21387945	178727.73
western_europe-Monsanto-14_SRR1946407	19483841	162816.14
western_europe-Monsanto-15_SRR1945552	16259172	135869.29
western_europe-Monsanto-1_SRR1946464	7161758	59847.02
western_europe-Monsanto-2_SRR1946372	15399476	128685.26
western_europe-Monsanto-3_SRR1945568	21045538	175866.41
western_europe-Monsanto-4_SRR1945891	19333214	161557.43
western_europe-Monsanto-5_SRR1946055	12240368	102286.27

western_europe-Monsanto-6_SRR1946116	11464228	95800.48
western_europe-Monsanto-7_SRR1946460	10741251	89758.95
western_europe-Monsanto-8_SRR1945557	14674892	122630.3
western_europe-Monsanto-9_SRR1945438	18291432	152851.81

1001 Genomes Consortium, 2016 1,135 Genomes Reveal the Global Pattern of Polymorphism in Arabidopsis thaliana. Cell 166: 481–491. https://doi.org/10.1016/j.cell.2016.05.063

Alkan C., B. P. Coe, and E. E. Eichler, 2011 Genome structural variation discovery and genotyping. Nat. Rev. Genet. 12: 363–376.

Amundson K. R., B. Ordoñez, M. Santayana, E. H. Tan, I. M. Henry, *et al.*, 2020a Genomic Outcomes of Haploid Induction Crosses in Potato (Solanum tuberosum L.). Genetics 214: 369–380. https://doi.org/10.1534/genetics.119.302843

Amundson K. R., B. Ordoñez, M. Santayana, M. L. Nganga, I. M. Henry, *et al.*, 2020b Rare instances of haploid inducer DNA in potato dihaploids and ploidy-dependent genome instability. BioRxiv.

Anaconda, Anaconda.

Bastiaanse H., M. Zinkgraf, C. Canning, H. Tsai, M. Lieberman, *et al.*, 2019 A comprehensive genomic scan reveals gene dosage balance impacts on quantitative traits in Populus trees. Proc. Natl. Acad. Sci. U. S. A. https://doi.org/10.1073/pnas.1903229116

Belling J., and A. F. Blakeslee, 1924 The Configurations and Sizes of the Chromosomes in the Trivalents of 25-Chromosome Daturas. Proc. Natl. Acad. Sci. U. S. A. 10: 116–120. https://doi.org/10.1073/pnas.10.3.116

Benjamini Y., and Y. Hochberg, 1995 Controlling the false discovery rate: a practical and powerful approach to multiple testing. J. R. Stat. Soc. Series B Stat. Methodol. 289–300.

Boer J. M. de, E. Datema, X. Tang, T. J. A. Borm, E. H. Bakker, *et al.*, 2015 Homologues of potato chromosome 5 show variable collinearity in the euchromatin, but dramatic absence of sequence similarity in the pericentromeric heterochromatin. BMC Genomics 16: 374. https://doi.org/10.1186/s12864-015-1578-1

Braz G. T., L. He, H. Zhao, T. Zhang, K. Semrau, *et al.*, 2018 Comparative Oligo-FISH Mapping: An Efficient and Powerful Methodology To Reveal Karyotypic and Chromosomal Evolution. Genetics 208: 513–523. https://doi.org/10.1534/genetics.117.300344

Braz G. T., F. Yu, L. do Vale Martins, and J. Jiang, 2020 Fluorescent In Situ Hybridization Using Oligonucleotide-Based Probes. Methods Mol. Biol. 2148: 71–83. https://doi.org/10.1007/978-1-0716-0623-0_4

Bridges C. B., 1923 The translocation of a section of chromosome II upon chromosome III in Drosophila. Anat. Rec. 24: 426–427.

Brown C. R., 1993 Outcrossing rate in cultivated autotetraploid potato. Am. Potato J. 70: 725–734. https://doi.org/10.1007/BF02848678

Burnham C. R., 1956 Chromosomal interchanges in plants. Bot. Rev. 22: 419–552. https://doi.org/10.1007/BF02872484

Cabanettes F., and C. Klopp, 2018 D-GENIES: dot plot large genomes in an interactive, efficient and simple way. PeerJ 6: e4958. https://doi.org/10.7717/peerj.4958

Chen W., R. Ullmann, C. Langnick, C. Menzel, Z. Wotschofsky, *et al.*, 2010 Breakpoint analysis of

balanced chromosome rearrangements by next-generation paired-end sequencing. Eur. J. Hum. Genet. 18: 539–543. https://doi.org/10.1038/ejhg.2009.211

Comai L., 2005 The advantages and disadvantages of being polyploid. Nat. Rev. Genet.

Cremer T., P. Lichter, J. Borden, D. C. Ward, and L. Manuelidis, 1988 Detection of chromosome aberrations in metaphase and interphase tumor cells by in situ hybridization using chromosome-specific library probes. Hum. Genet. 80: 235–246. https://doi.org/10.1007/bf01790091

DePristo M. A., E. Banks, R. Poplin, K. V. Garimella, J. R. Maguire, *et al.*, 2011 A framework for variation discovery and genotyping using next-generation DNA sequencing data. Nat. Genet. 43: 491–498.

Díaz A., M. Zikhali, A. S. Turner, P. Isaac, and D. A. Laurie, 2012 Copy number variation affecting the Photoperiod-B1 and Vernalization-A1 genes is associated with altered flowering time in wheat (Triticum aestivum). PLoS One 7: e33234. https://doi.org/10.1371/journal.pone.0033234

Falque M., K. Jebreen, E. Paux, C. Knaak, S. Mezmouk, *et al.*, 2019 CNVmap: A Method and Software To Detect and Map Copy Number Variants from Segregation Data. Genetics. https://doi.org/10.1534/genetics.119.302881

Gong Z., Y. Wu, A. Koblízková, G. A. Torres, K. Wang, *et al.*, 2012 Repeatless and repeat-based centromeres in potato: implications for centromere evolution. Plant Cell 24: 3559–3574. https://doi.org/10.1105/tpc.112.100511

Han Y., T. Zhang, P. Thammapichai, Y. Weng, and J. Jiang, 2015 Chromosome-Specific Painting in Cucumis Species Using Bulked Oligonucleotides. Genetics 200: 771–779. https://doi.org/10.1534/genetics.115.177642

Hardigan M. A., E. Crisovan, J. P. Hamilton, J. Kim, P. Laimbeer, *et al.*, 2016 Genome Reduction Uncovers a Large Dispensable Genome and Adaptive Role for Copy Number Variation in Asexually Propagated Solanum tuberosum. Plant Cell 28: 388–405.

Hardigan M. A., F. P. E. Laimbeer, L. Newton, E. Crisovan, J. P. Hamilton, *et al.*, 2017 Genome diversity of tuber-bearing Solanum uncovers complex evolutionary history and targets of domestication in the cultivated potato. Proc. Natl. Acad. Sci. U. S. A. https://doi.org/10.1073/pnas.1714380114

He L., G. T. Braz, G. A. Torres, and J. Jiang, 2018 Chromosome painting in meiosis reveals pairing of specific chromosomes in polyploid Solanum species. Chromosoma 127: 505–513. https://doi.org/10.1007/s00412-018-0682-9

Henry I. M., M. S. Zinkgraf, A. T. Groover, and L. Comai, 2015 A System for Dosage-Based Functional Genomics in Poplar. Plant Cell 27: 2370–2383. https://doi.org/10.1105/tpc.15.00349

Hinds D. A., A. P. Kloek, M. Jen, X. Chen, and K. A. Frazer, 2006 Common deletions and SNPs are in linkage disequilibrium in the human genome. Nat. Genet. 38: 82–85. https://doi.org/10.1038/ng1695

Hunter J. D., 2007 Matplotlib: A 2D Graphics Environment. Comput. Sci. Eng. 9: 90–95. https://doi.org/10.1109/MCSE.2007.55

Khush G. S., 1973 *Cytogenetics of aneuploids*. Academic Press, New York.

Li H., 2013 Aligning sequence reads, clone sequences and assembly contigs with BWA-MEM. arXiv [q-bio.GN].

Locke D. P., A. J. Sharp, S. A. McCarroll, S. D. McGrath, T. L. Newman, *et al.*, 2006 Linkage disequilibrium and heritability of copy-number polymorphisms within duplicated regions of the

human genome. Am. J. Hum. Genet. 79: 275–290. https://doi.org/10.1086/505653

Maron L. G., C. T. Guimarães, M. Kirst, P. S. Albert, J. A. Birchler, *et al.*, 2013 Aluminum tolerance in maize is associated with higher MATE1 gene copy number. Proc. Natl. Acad. Sci. U. S. A. 110: 5241–5246. https://doi.org/10.1073/pnas.1220766110

McClintock B., 1930 A CYTOLOGICAL DEMONSTRATION OF THE LOCATION OF AN INTERCHANGE BETWEEN TWO NON-HOMOLOGOUS CHROMOSOMES OF ZEA MAYS. Proc. Natl. Acad. Sci. U. S. A. 16: 791–796.

Muller H. J., 1929 The First Cytological Demonstration of a Translocation in Drosophila. Am. Nat. 63: 481–486. https://doi.org/10.1086/280282

Negri L. H., PeakUtils

Peloquin S. J., S. H. Jansky, and G. L. Yerk, 1989 Potato cytogenetics and germplasm utilization. Am. Potato J. 66: 629–638. https://doi.org/10.1007/BF02853983

Perkel J. M., 2018 Why Jupyter is data scientists' computational notebook of choice. Nature 563: 145–146. https://doi.org/10.1038/d41586-018-07196-1

Rieseberg L. H., 2001 Chromosomal rearrangements and speciation. Trends Ecol. Evol. 16: 351–358. https://doi.org/10.1016/s0169-5347(01)02187-5

Rokka V.-M., 2009 Potato Haploids and Breeding, pp. 199–208 in *Advances in Haploid Production in Higher Plants*, edited by Touraev A., Forster B. P., Jain S. M. Springer Netherlands, Dordrecht.

Sedlazeck F. J., P. Rescheneder, M. Smolka, H. Fang, M. Nattestad, *et al.*, 2018 Accurate detection of complex structural variations using single-molecule sequencing. Nat. Methods 15: 461–468.

https://doi.org/10.1038/s41592-018-0001-7

Swanson-Wagner R. A., S. R. Eichten, S. Kumari, P. Tiffin, J. C. Stein, *et al.*, 2010 Pervasive gene content variation and copy number variation in maize and its undomesticated progenitor. Genome Res. 20: 1689–1699.

Velásquez A. C., E. Mihovilovich, and M. Bonierbale, 2007 Genetic characterization and mapping of major gene resistance to potato leafroll virus in Solanumtuberosum ssp. andigena. Theor. Appl. Genet. 114: 1051–1058. https://doi.org/10.1007/s00122-006-0498-5

Waskom M., An introduction to seaborn — seaborn 0.10.0 documentation. Seaborn.

Zhang H., A. Koblížková, K. Wang, Z. Gong, L. Oliveira, *et al.*, 2014 Boom-Bust Turnovers of Megabase-Sized Centromeric DNA in Solanum Species: Rapid Evolution of DNA Sequences Associated with Centromeres. Plant Cell 26: 1436–1447. https://doi.org/10.1105/tpc.114.123877

Zhang T., G. Liu, H. Zhao, G. T. Braz, and J. Jiang, 2021 Chorus2: design of genome-scale oligonucleotide-based probes for fluorescence in situ hybridization. Plant Biotechnol. J. https://doi.org/10.1111/pbi.13610